Synthesis and Characterization of a Novel Silicone Containing Vinylic Macromonomer and Its Uses in the Preparation of Poly (silicone-*co*-styrene-*co*-butylacrylate) with Montmorillonite Nanocomposite Emulsion

Hamid Javaherian Naghash, Farhad Hajati

Department of Chemistry, Islamic Azad University, Shahreza Branch, Shahreza, Isfahan, I. R. Iran

Received 5 September 2010; accepted 30 March 2011
DOI 10.1002/app.34601
Published online 12 August 2011 in Wiley Online Library (wileyonlinelibrary.com).

ABSTRACT: A new silicone containing macromonomer, 4-(methacrylamido) phenoxy polymethylhydrosiloxane (4-MPMHS) with a vinyl group, was successfully synthesized. Then poly (silicone-*co*-styrene-*co*-butylacrylate) with montmorillonite, P (Si-*co*-St-*co*-BA) with MMT nanocomposite emulsion was prepared by *in situ* intercalative emulsion polymerization of styrene (St), butyl acrylate (BA), and 4-MPMHS, in the presence of organic modified montmorillonite (OMMT) with different OMMT contents (0, 0.5, 1.0, 1.5, and 2 wt %). Potassium persulphate (KPS) was used as an initiator and sodium lauryl sulfoacetate (SLSA) and nonyl phenol ethylene oxide—40 U (NP-40) were used as anionic and nonionic emulsifiers, respectively. The resulting macromonomer was characterized by elemental analysis, Fourier transformer infrared (FT-IR), proton (^{1}H NMR), and carbon (^{13}C NMR) nuclear magnetic resonance spectroscopes. The OMMT was characterized by FT-IR and X-ray diffraction (XRD). The nanocomposite emulsions were characterized by using Fourier Transform infrared spectroscopy (FT-IR), laser light scattering, and surface tension method. Thermal properties of the copolymers were studied using thermogravimetric analysis (TGA) and differential scanning calorimetry (DSC) and then the effects of OMMT percent on the water absorption ratio and drying speed were examined. Results showed that OMMT could improve the properties of emulsion. In other words, the properties of nanocomposite emulsions were better when compared with those of the silicone-acrylate emulsion. The property of nanocomposite emulsion containing 1 wt % OMMT was the best one, and the following advantages were obtained: smaller particle size, faster drying speed, smaller surface tension, and improved water resistance by the incorporation of OMMT. © 2011 Wiley Periodicals, Inc. J Appl Polym Sci 123: 1227–1237, 2012

Key words: silicones; morphology; emulsion polymerization; nanocomposites

INTRODUCTION

Copolymers of silicone, acrylics, and styrene (St) have many specific features such as good film-forming, gloss, transparency, and mechanical properties. These copolymers and their corresponding products have been widely used as coatings, paints, adhesives, textile coatings, and hide finishes, because of their various advantages, such as good film forming property, high adhesive strength, resistance to high and low temperature, chemicals, water, weather, ultraviolet, and anticontamination.[1–10] However, the application of poly (silicone-styrene-acrylics) emulsion was limited because of the high price of silicone. The polymer/layered silicate (PLS) nanocomposite have drawn much research attention because they effectuate in improving material properties by the presence of a small amount of layered silicate, and promise superior or unique properties in comparison with those of the conventional polymer composites, including increased modulus, decreased thermal expansion coefficient, increased heat distortion temperature, reduced gas permeability,[11–14] better fire-retardant properties,[15,16] enhanced ionic conductivity, low flammability, increased solvent resistance, lower material cost, and the ease of preparation and processing.[17–22] PLS nanocomposite can be prepared in four main ways: solution intercalation, *in situ* intercalative polymerization, melts interaction, and template synthesis.[23] Montmorillonite (MMT) is a kind of layered silicate, which was used usually. It has been particularly important in forming effective polymer nanocomposite. It belongs to a smectite group of clay minerals that has 2 : 1 type of layer structure, in which a central alumina octahedral sheet is sandwiched between two silica tetrahedral sheets.[24] Polyacrylate/OMMT nanocomposites have been made *in situ* polymerization and their properties have been reported.[25] Although there are many reports for PLS nanocomposite. However, there has been few studies on the

Correspondence to: H. J. Naghash (Javaherian@iaush.ac.ir).

PLS nanocomposite emulsion. In this article, we prepared the poly (silicone-*co*-styrene-*co*-butylacrylate) and montmorillonite nanocomposite emulsion with different OMMT contents (0, 0.5, 1.0, 1.5, and 2 wt %) and organosilicone (1.50, 3.0, and 5.0 wt %) via *in situ* intercalative polymerization. The properties of nanocomposite emulsion and influence of different amounts of OMMT and organosilicone on the nanocomposite emulsion were examined.

EXPERIMENTAL

Materials

The monomers St (Aldrich) and BA (Aldrich) were freed from the inhibitor by shaking with 10% aqueous NaOH, washing with distilled water and drying over Na_2SO_4. They were then distilled under reduced pressure before use and stored at −15°C to avoid thermal polymerization. The initiator KPS (Merck); buffer, $NaHCO_3$ (Merck); and the emulsifiers sodium lauryl sulfoacetate (SLSA) and nonyl phenol ethylene oxide—40 U (NP-40) were purchased from Henkel, Germany and were used as received. The antifoam, EFKA-2526 was kindly supplied by EFKA, Holland. Sodium montmorillonite (MMT) is supplied by Zhejiang Geologic Institute. The 4-aminophenol (4-APh), methacryloyl chloride (MAC) polymethylhydrosiloxane (PMHS), triethylamine (TEA), tetrahydrofuran, cetyl trimethylammonium bromide (CTAB) sodium silicate (Na_2SiO_3), and ethylene glycol (inhibitor) were supplied by Merck Chemicals, Darmstadt, Germany and were used directly without further purification. Polyvinyl alcohol (PVA, protective colloid) is supplied by Sichuan Vinylon Factory. Double-distilled and deionized (DDI) water was used throughout.

Synthesis of 4-(methacrylamido) phenoxy polymethylhydrosiloxane (4-MPMHS)

A dried 50-mL three-necked round bottom flask, purged with nitrogen. The flask was equipped with a reflux condenser, a dropping funnel, and nitrogen inlet and contained 0.22 g, (2.00 mmoL) 4-APh, 10 mL tetrahydrofuran (THF) and 0.28 mL (2 mmoL) triethylamine (TEA). To synthesize the 4-MPMHS the content of the flask was stirred for 3 h. Then, 4.52 g (2.00 mmoL) polymethylhydrosiloxane (PMHS) which dissolved in 8 mL THF was added drop-wise at room temperature under nitrogen atmosphere. The reaction mixture was refluxed for 4 h and then 30 min at room temperature to obtain 4-aminophenoxypolymethylhydrosiloxane (4-APMHS). The viscous crude product was recovered after removing the solvent using an evaporator. The reaction progressed with addition of a solution of 0.20 mL

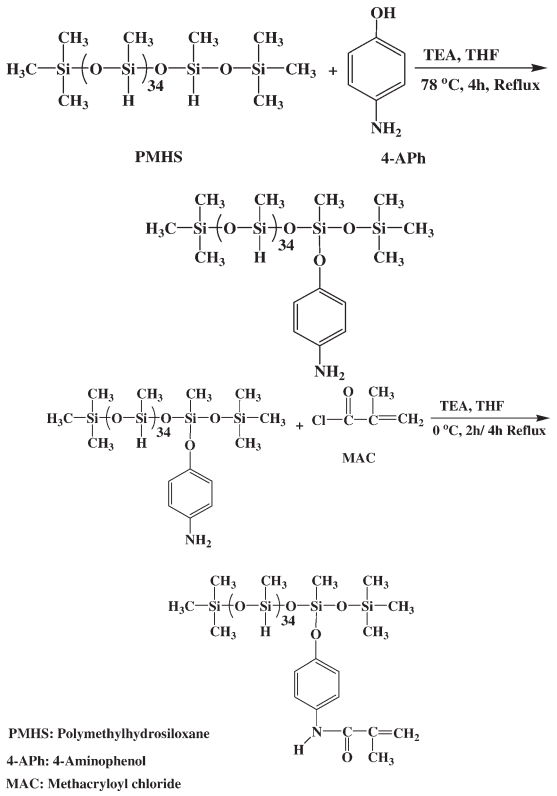

Scheme 1 Preparation of 4-MPMHS.

(2.00 mmoL) MAC and 2 mL THF to the 4-APMHS first in an ice bath for 2 h and then was refluxed for 3 h to produce macromonomer. Use of TEA promotes the desirable condensation between polymethylhydrosiloxane-H and 4-Aminophenol-OH and avoids the self-condensation of silicone intermediates. After evaporation of THF, the product was dried on vacuum, yielding 4.94 g with 86%. The reaction path is given in Scheme 1.

Preparation of OMMT

The required weights of MMT and distilled water were added into a three-necked flask. Sodium silicate was added to adjust pH to 11. The mixture was allowed stand for 1 day after stirring for 4 h, at room temperature. The supernatant of the mixture was subsequently poured into another flask, and followed by addition of the required weights of CTAB. The blend was heated up to 90°C and stirred at the same temperature for 2 h. After that, the blend was washed using distilled water to make it free from bromide ions and filtrated with pump down. Finally, the resultant was dried in a vacuum oven and ground to 300 meshes.

Preparation of emulsion

The emulsions were prepared according to Ref. 26. Briefly the given weights of St, BA, and OMMT

TABLE I
Recipe for the Emulsion Copolymerization

Ingredients	Charge (g)
St	49.00
n-BA	50.00
Buffer: $NaHCO_3$	0.60
Initiator: KPS	0.84
Demineralized water	90.00
Nonionic emulsifier: Nonyl phenol ethylene oxide – 40 U (NP-40)	4.00
Anionic emulsifier: sodium lauryl sulphoacetate (SLSA)	4.00
Protective colloid: PVA	0.20
Inhibitor: ethylene glycol (EG)	0.50

were premixed for 1 day to get mixture I. Initiator was dissolved in distilled water to make 10% of solution. Two-thirds of the required weights of distilled water, emulsifier, and total protective colloid and buffer agent were put into a dried three-necked flask equipped with a stirrer, a thermometer, and a condenser. The mixture was heated to 52°C, then, the mixture I was added into the flask. The blend was stirred vigorously at 52–55°C for 10 min to obtain preemulsion. The 1/8 of the preemulsion were taken into another flask and heated to 75°C. Then, 1/3 of given amounts of initiator solution, emulsifier, and distilled water were added to the flask. The blend was reacted for 30 min and a seed emulsion was obtained. Two-thirds of initiator solution was added to remaining 7/8 of the preemulsion. The preemulsion with initiator and 4-MPMHS were, respectively, dropped into the seed emulsion at the same time in about 2 h, and kept at 75°C for another 2 h. Then, the system was heated up to (81 ± 1)°C and maintained at this temperature for 1.5 h. Finally, a kind of white fluid P (Si-*co*-St-*co*-BA) with MMT nanocomposite emulsion was obtained.

To determine the conversion percent during the polymerization process, it was necessary to withdraw samples at various intervals from the reaction vessel. These samples are relatively small so that the overall composition in the reactor is not seriously affected; once a sample is removed and put in a watch glass, polymerization is terminated by the addition of 7 ppm hydroquinone. Then, two drops of ethanol was added to the sample as a coagulant and the contents of the watch glass were evaporated at room temperature and then dried to a constant weight in a vacuum oven. The conversion percent was determined gravimetrically. The number of polymer particles per unit volume of water (N_T) was calculated from the monomer conversion X_M and the volume average diameter of the polymer particles, d_v was determined by a scanning electron microscope, using the following equations:

$$d^3{}_\upsilon = \frac{\sum n_i d^3{}_\upsilon}{\sum n_i}, \quad (1)$$

$$N_T = \frac{6M_o X_M}{\pi d^3{}_\upsilon \rho_p}, \quad (2)$$

where M_0 is the initial monomer concentration per mL and ρ_p is the density of the polymer (g cm^{-3}).[27–29] The volume average diameter ($d^3{}_\upsilon$) of the lattices was found to be 1.4×10^{-14}, 8.4×10^{-15}, and 1.3×10^{-14} mL for P (St-*co*-BA), P (St-*co*-BA) with OMMT and P (St-*co*-BA-*co*-Si) with OMMT, respectively. A typical recipe for the preparation of a 50% solid product and the contents of Si and OMMT of emulsion are given in Tables I and II and the process is given in Scheme 2, respectively.

Preparation of film

Emulsions were laid on the polytef mold and formed film at room temperature for 3 days. Then, the films were further heated in a vacuum oven at 100°C for 3 h.

Polymer characterization

Fourier-transform infrared (FTIR) spectroscopy analysis was performed with a Nicolet Impact 400D Model spectrophotometer (Nicolet Impact, Madison, USA) using KBr pellets. The spectra were obtained over the wave number range 4000–500 cm^{-1} at a resolution of 2 cm^{-1} using an MCT detector with coaddition of 64 scans. Scanning electron micrographs were taken on a JEOL-JXA 840 A SEM (JEOL, Boston, USA). The specimens were prepared for SEM by freeze-fracturing in liquid nitrogen and the application of a gold coating of ~ 300 Å with an

TABLE II
Content of 4-MPMHS and OMMT of Emulsion

No. of samples	Si (%)	OMMT (%)	No. of samples	Si (%)	OMMT (%)	No. of samples	Si (%)	OMMT (%)
1	1.5	0.0	6	3.0	0.0	11	5.0	0.0
2	1.5	0.5	7	3.0	0.5	12	5.0	0.5
3	1.5	1.0	8	3.0	1.0	13	5.0	1.0
4	1.5	1.5	9	3.0	1.5	14	5.0	1.5
5	1.5	2.0	10	3.0	2.0	15	5.0	2.0

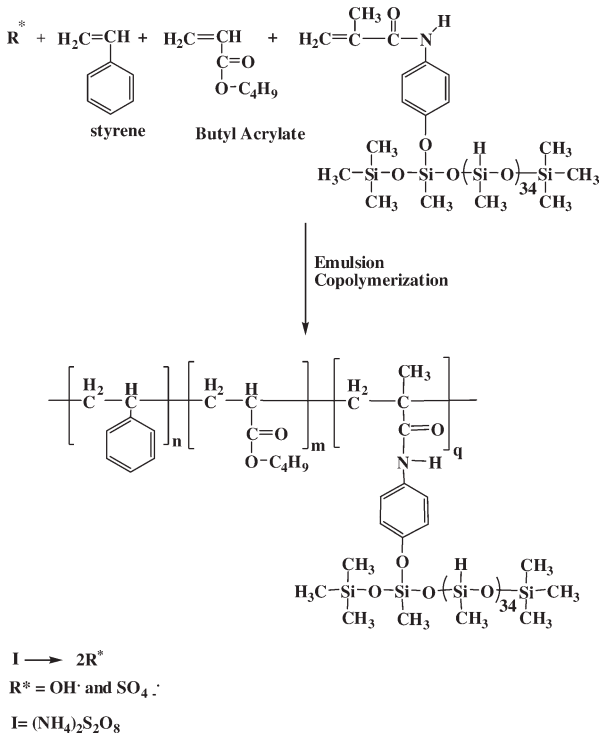

Scheme 2 Emulsion polymerization process.

Edwards S 150 B sputter coater. The X-ray diffraction (XRD) analysis was performed using a Japanese D/max-rA X-ray diffractometer (Cu Kα radiation, λ = 0.154 nm, 40 kV, 70 mA). Laser light scattering was carried out using a Mastersizer-2000 of Malvern Instruments (Worcestershire, UK). The surface tension was measured using German du Nouy surface tension equipment. The measured temperature was established at (25 ± 0.1)°C. TGA measurements of copolymers were carried out by a Dupont TGA 951 under nitrogen atmosphere at a heating rate of 10°C min^{-1}. Differential scanning calorimetry (DSC) thermograms were taken on a Mettler TA 4000 Model apparatus at a heating rate of 10°C min^{-1}. The T_g was taken at the onset of the corresponding heat capacity jump. The samples were cooled to −150°C, equilibrated for 3 min, and then heated to 250°C at a constant heating rate of 5°C min^{-1}, at a frequency of 10 Hz, under a nitrogen atmosphere. (^{13}C, ^{1}H) nuclear magnetic resonance (NMR) spectra measurements were recorded on a Bruker AV300 MHz spectrometer (4 mm specimen tube). The water absorption was tested by weighing the film, which was submerged in distilled water for 2 days at room temperature Elemental analysis was performed by elementar Vario EL III and dried with a paper towel before weighing. The water absorption was calculated from the following equation:

$$\text{Water absorption } (\%) = [(w_1 - w_0)/w_0], \quad (3)$$

where w_0 is the weight of dried film and w_1 is the weight of the film after absorbing water. The solid content of emulsion was obtained by weighing the emulsion on an electronic balance before and after the emulsions was dried at 120°C for 20 min. The solid content T was calculated by the equation:

$$T = (m_2 - m_0)/(m_1 - m_0), \quad (4)$$

where m_0 is the weight of the vessel, m_1 is the weight of the emulsion and the vessel, m_2 is the weight of the vessel and dried emulsion. The solid contents of emulsion came out to be (50 ± 0.2)%.

RESULTS AND DISCUSSION

FTIR spectrum of 4-MPMHS

Figure 1 shows the typical FTIR spectra of (A) PMHS, (B) 4-APh, (C) 4-APMHS, (D) MAC, and (E) 4-MPMHS. It can be seen from Figure 1(A) that there are strong absorption peaks at 2965, 2169, 1264, 1092, and 891 cm^{-1}, which are ascribed to the vibration of —CH_3, Si—H, Si—CH_3, and Si—O—R. The same peaks are present in Figure 1(C). In addition, there are two peaks at 3280 and 3342 cm^{-1}, which are ascribed to the vibration of —NH_2 indicating that the —NH group of 4-APh reacted with PMHS [Fig. 1(C)]. Figure 1(E) shows a weak peak at 3311 cm^{-1}, which is ascribed to the vibration of —NH. Also there are peaks at 2966, 2169, 1263, 1095, and 892 cm^{-1}, which are attributed to the vibration of —CH_3, Si—H, Si—CH_3, and Si—O—R. The aforementioned peaks have demonstrated that 4-MPMHS has been synthesized successfully.

NMR analysis of 4-APMHS

^{1}H NMR is the most useful for the measurement of hydrogen chemical environment because of its high sensitivity to hydrogen bond strength, while the area of apex evidently reflects the abundance of hydrogen in different chemical shift.[30] The ^{1}H NMR of 4-APMHS is shown in Figure 2, it can be seen that all the relevant peaks of oligomer could be found in the mentioned Figure, the peaks at −0.5–0.4 ppm result from the group of —CH_3 in the chain of Si—O—Si in the molecule of 4-APMHS. The signal of the —NH_2 resonance has been obtained at 3.6 ppm. Also a signal of the Si—H resonance has been obtained at 4.7 ppm and another two small peaks have been observed at 6.9–7.5 ppm which belongs to H of benzene ring in the molecule of 4-APMHS. Figure 3 indicates the ^{13}C NMR spectrum of 4-APMHS. The number of carbons in the 4-APMHS is compatible with the number of spectrums.

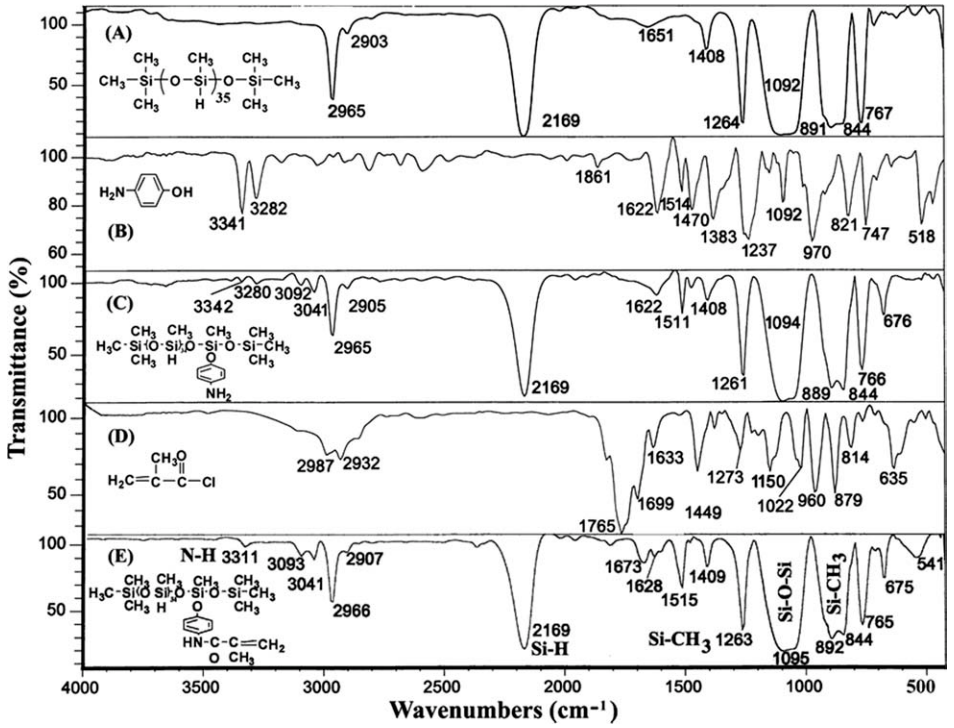

Figure 1 FTIR spectra of (A) PMHS, (B) 4-APh, (C) 4-APMHS, (D) MAC, and (E) 4-MPMHS.

NMR analysis of 4-MPMHS

The ^{1}H NMR of 4-MPMHS is shown in Figure 4, it can be seen that all the relevant peaks of oligomer could be found in the mentioned Figure, the peaks at −0.8–1.0 ppm result from the group of —CH_3 in the chain of Si—O—Si in the molecule of 4-MPMHS. The signals of the —CH_3 resonance have been obtained at 2 ppm. Also two small peaks have been observed at 5.0–6.0 ppm and another two peaks at 6.8–7.5 ppm which belong to vinyl group (CH_2=CH—) and —CH_2, in the molecule of 4-MPMHSrespectively. A small peak at 7.5–7.7 ppm shows the —NH bonding of amide group.

Figure 5 indicates the ^{13}C NMR spectrum of 4-MPMHS. The number of carbons in the 4-MPMHS is compatible with the number of spectrums.

Elemental analysis of 4-APMHS and 4-MPMHS

The elemental analysis results are in good agreement with calculated percentages of carbon, hydrogen and

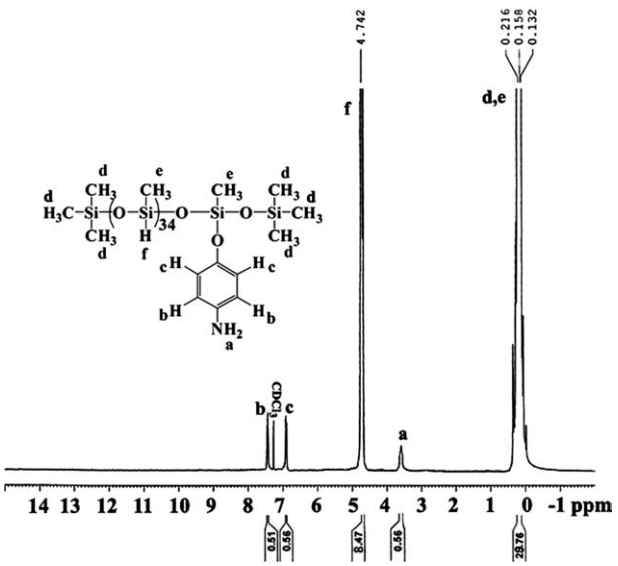

Figure 2 ^{1}H NMR spectrum of 4-APMHS.

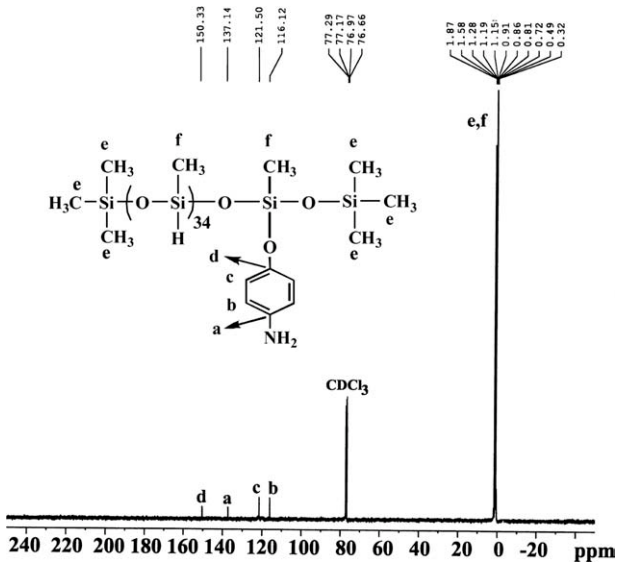

Figure 3 ^{13}C NMR spectrum of 4-APMHS.

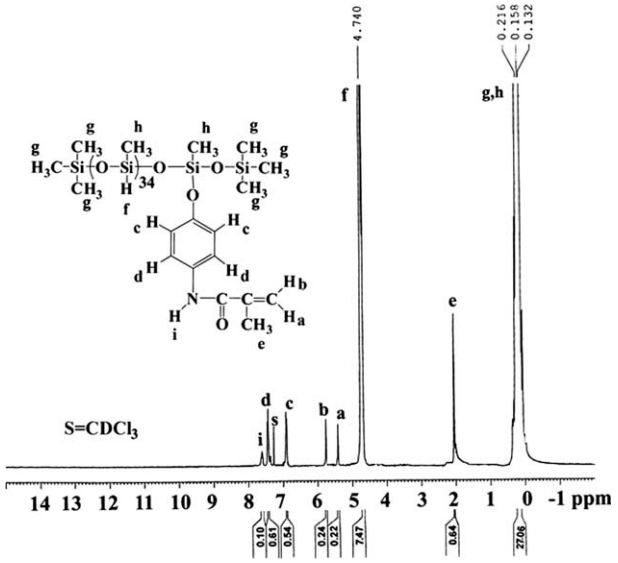

Figure 4 ^{1}H NMR spectrum of 4-MPMHS.

nitrogen contents in the 4-APMHS and 4-MPMHS (Table III).

FTIR spectrum of MMT and OMMT

Figure 6 illustrates the FTIR spectrum of (A) MMT and (B) OMMT. Unmodified MMT is evident from some groups of materials with absorption peaks fewer than 1200 cm^{-1}. No specific difference is seen in absorption peaks at 1030 cm^{-1} belonging to Si—O in MMT or OMMT. Generally, the vibration of —CH of alkyl ammonium cations are obvious at 2800—3020 cm^{-1} and the peak of N^{+} $(CH_3)_3$ cation is seen at 1487 cm^{-1}. Accordingly, the MMT has been modified to OMMT.

Distance of MMT and OMMT layers

The distances between MMT layers and OMMT layers, were respectively, calculated with Bragg law[31]:

$$2d \sin \theta = n \lambda, \quad (5)$$

where λ is the wavelength of the X-ray ($\lambda = 0.154$ nm), d is the interspaced distance, and θ is the angle of incident radiation (Fig. 7). It can be obtained that the distance between MMT layers are 1.262 nm, and the distance between OMMT layers are 1.471 nm. The results showed that organic CTAB has been intercalated between MMT layers.

FTIR spectrum of poly (St-*co*-BA-*co*-Si) and MMT nanocomposite emulsion

Figure 8 illustrates the FTIR spectrum of (A) P (St-*co*-BA), (B) P (St-*co*-BA) with OMMT, and (C) P (St-*co*-BA-*co*-Si) with OMMT, respectively. It can be seen from Figure 8 (A) that there are strong absorption peaks at 2939, 2871, and 1730 cm^{-1}, which are ascribed to the vibration of —CH_3, —CH_2, and C=O. After addition with OMMT [see Fig. 8(B)], a new sharp peak appeared at 1257 cm^{-1}, which was attributed to OMMT absorption. In Figure 8(C) a new sharp peak appeared at 2165 cm^{-1}, which was attributed to Si—H absorption. The peaks at 1261 and 1036 cm^{-1} also belong to Si—CH_3 and Si—O—Si, absorptions. These indicated the presence of 4-MPMHS bond formation.

Particle size of the emulsion

The particle size and the distribution of particle size of the emulsions were measured by laser light scattering and are shown in Figure 9. The geometric mean diameter (d_g) was calculated according to the following equation[32]:

$$d_g = \exp[\Sigma(n_i \ln d_i)/N], \quad (6)$$

where n_i is the number of particles in group i, with a midpoint of size d_i, and $N = \Sigma n_i$, means the total number of particles. According to Figure 9(A–C) and eq. (6), it can be obtained that the d_g were 243, 204, and 235 nm for the emulsions containing 0, 1, and 2 wt % of OMMT, respectively. It is obvious that the particle size of nanocomposite emulsion was smaller than the nonmodified emulsion. In the polymerization process, a part of OMMT formed sheets under the effect of water and emulsifier. A part of monomers polymerized around the OMMT sheets and formed core-shell nanocomposite. This rendered an increase in number of emulsoid particle. Therefore, the emulsoid particle size decreased. However, if the content of OMMT exceeds the intercalative capacity

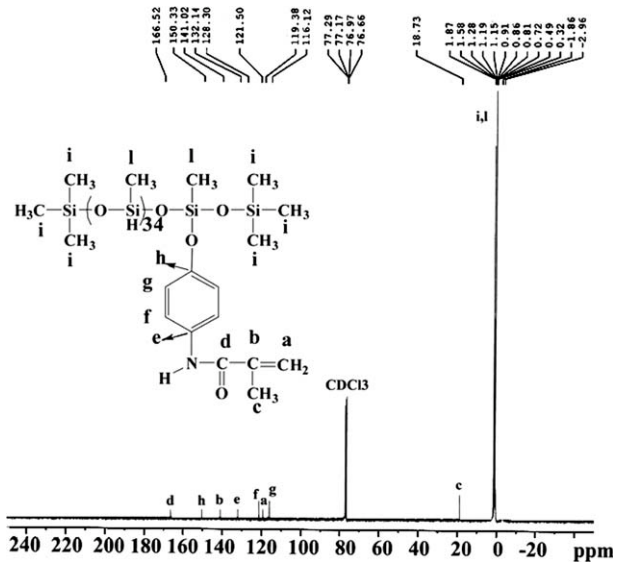

Figure 5 ^{13}C NMR spectrum of 4-MPMHS.

TABLE III
Elemental Analysis Data of 4-APMHS and 4-MPMHS

Formula		C (%)	H (%)	N (%)
4-APMHS: $C_{47}H_{163}N_1O_{37}Si_{37}$	Calculated	23.78	6.93	0.59
2373.70 g mol^{-1}	Found	24.00	6.92	0.57
4-MPMHS: $C_{51}H_{167}N_1O_{38}Si_{37}$	Calculated	25.22	6.94	0.57
2427.76 g mol^{-1}	Found	24.68	6.84	0.55

The 3-APMHS and 4-MPMHS samples were dried in vacua at 30°C for 10 h.

of monomer, emulsion will change into the blend of *in situ* composite and direct composite. The particle size was increased. Particle size distribution breadth (B) was calculated according to eq. (7).[33]

$$B = (D_{90} - D_{10})/D_{50}, \quad (7)$$

where D_{90}, D_{50}, and D_{10} are the particle diameters for the 90th, 50th, and 10th cumulative mass percentiles, respectively. The particle size distribution breadth of emulsions containing 0, 1, and 2 wt % OMMT were 1.24 and 1.05, and 1.08, respectively. This shows that the particle size distribution of nanocomposite emulsion was narrower. This was because OMMT sheets are regular.

Morphologies of the P (St-*co*-BA), P (St-*co*-BA) with OMMT and P (St-*co*-BA- co-Si) with OMMT

The particle morphologies of the P (St-*co*-BA), P (St-*co*-BA) with OMMT and P (St-*co*-BA-*co*-Si) with OMMT were examined by SEM and TEM, respectively. The micrographs of SEM are shown in Figure 10(A–C) and the data are given in Table IV. According to these micrographs the P (St-*co*-BA-*co*-Si) with OMMT copolymers have low particle size compared to P (St-*co*-BA) samples and according to the previous works by increasing the OMMT percent the particle size increases in a linear manner and their size distributions get narrower. From the data of Table IV it is obvious that the number of polymer particles increase by increasing the conversion monomers to copolymers. On the other hand, the conventional TEM can directly provide more information in real space, in a localized area, and on morphology and defect structures and also it is necessary for determining the nature of the nanocomposites. Typical TEM image of P (St-*co*-BA-*co*-Si) with OMMT nanocomposite with different magnifications is shown in Figure 11(A–C) and these can be observed with the presence of several OMMT layers in the P (St-*co*-BA-*co*-Si) matrix, which indicates formation of nanocomposites. TEM micrographs also prove that most OMMT layers are dispersed homogeneously into the polymer matrix, although some clusters or agglomerated particles are detected.

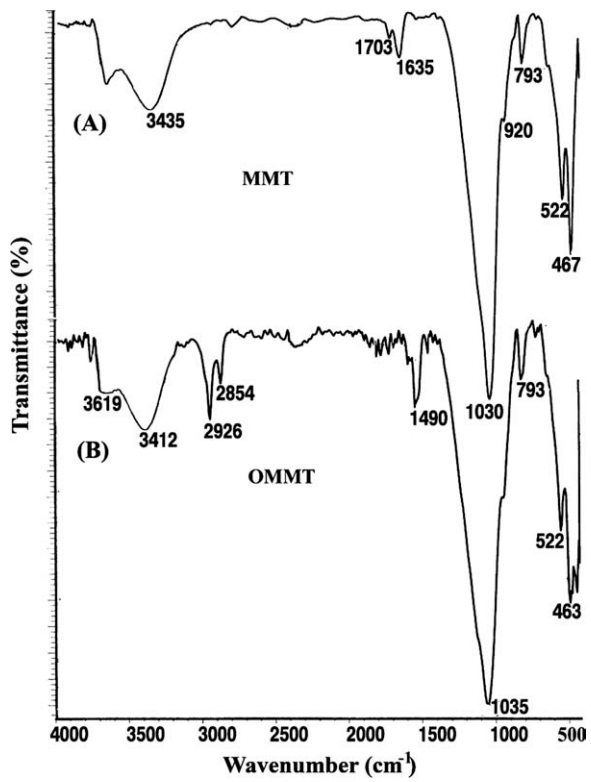

Figure 6 FTIR spectra of (A) MMT and (B) OMMT.

Water absorption ratio of the P (St-*co*-BA-*co*-Si) with OMMT films

The water absorption ratio of the P (St-*co*-BA-*co*-Si) with OMMT films is an important evidence of hydrophobicity. As shown in Table V, the film water

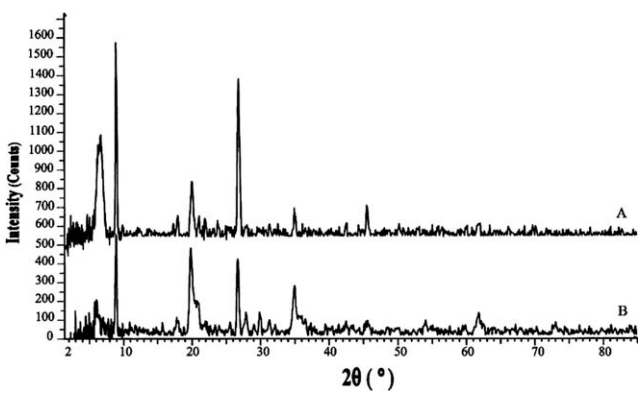

Figure 7 XRD patterns of (A) MMT and (B) OMMT.

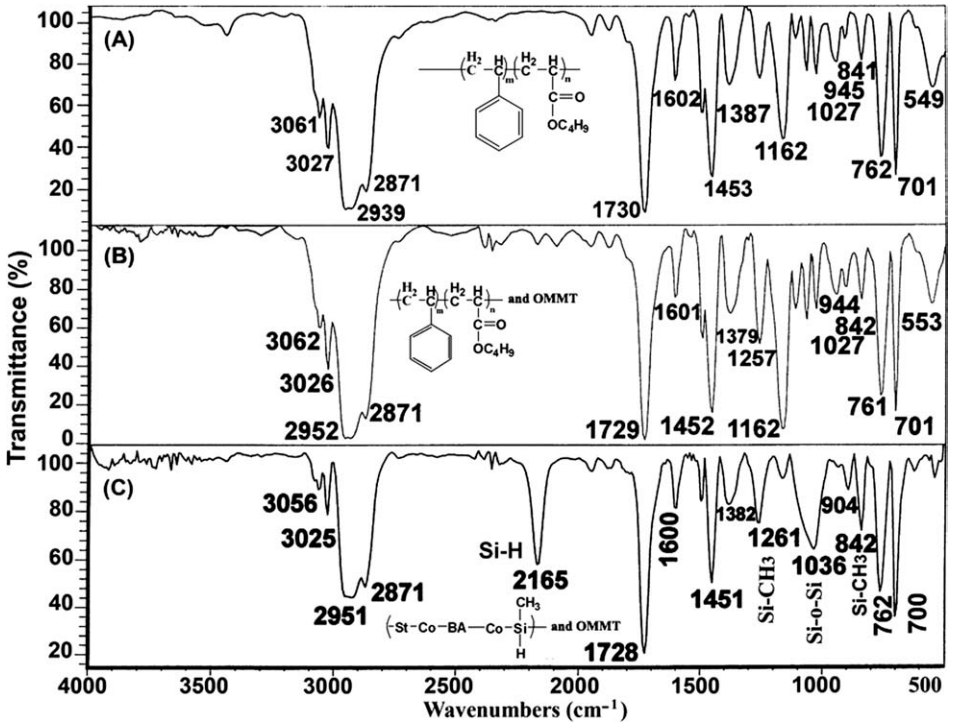

Figure 8 FTIR spectra of (A) P (St-*co*-BA), (B) P (St-*co*-BA) with OMMT and (C) P (St-*co*-BA-*co*-Si) with OMMT.

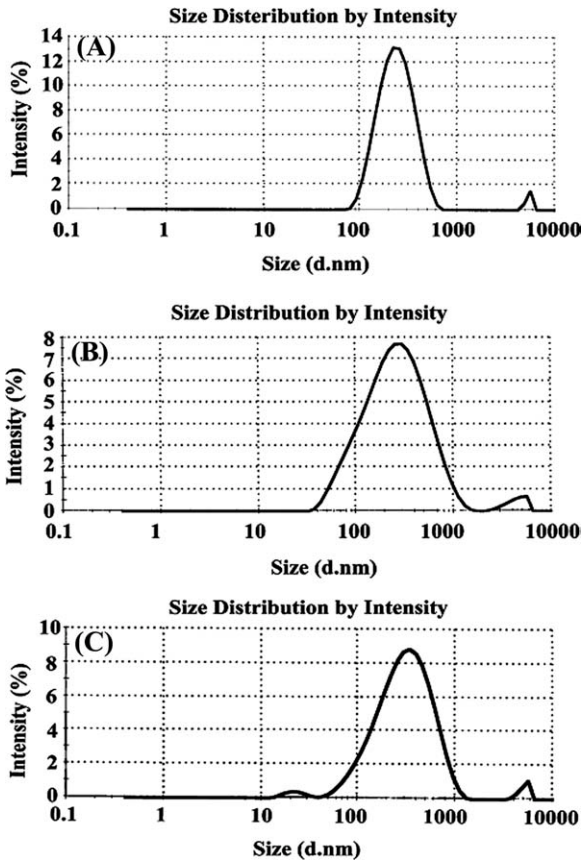

Figure 9 Laser light scattering graphs of the emulsion containing (A) 5 wt % 4- MPMHS and 0 wt % OMMT, (B) 5 wt % 4-MPMHS and 1 wt % OMMT, and (C) 5 wt % 4-MPMHS and 2 wt % OMMT.

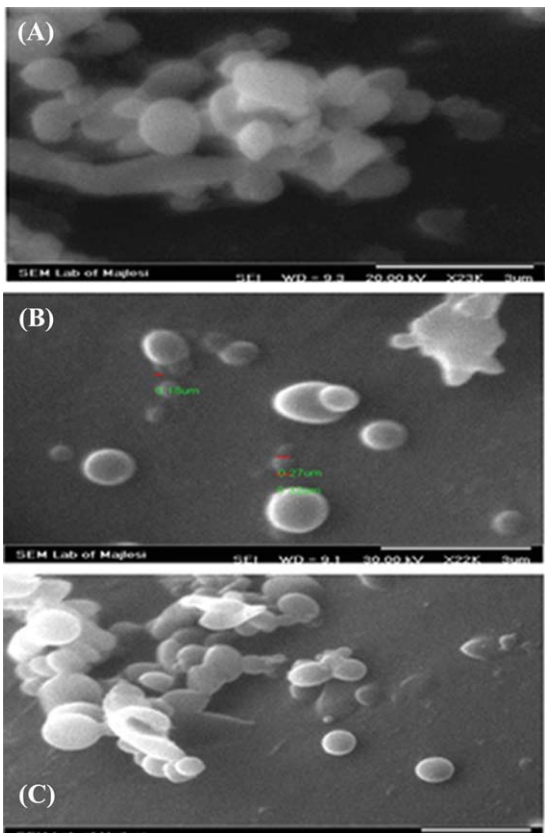

Figure 10 SEM micrographs of (A) P (St-*co*-BA), (B) P (St-*co*-BA) with OMMT and (C) P (St-*co*-BA- *co*-Si) with OMMT at 81°C.[Color figure can be viewed in the online issue, which is available at wileyonlinelibrary.com.]

TABLE IV
Morphologies of P (St-*co*-BA), P (St-*co*-BA) with OMMT and P (St-*co*-BA-*co*-Si) with OMMT

P(St/BA)	X_M	32.00	40.00	49.00	58.00	68.00	86.00	95.00
	$N_{T\times}10^{15}$	2.20	2.70	3.30	3.90	4.60	5.80	6.40
P(St/BA) and OMMT	X_M	27.00	34.00	45.00	52.00	66.00	79.00	89.00
	$N_{T\times}10^{15}$	1.82	2.30	3.00	3.52	4.50	5.40	6.00
P(St/BA/Si) and OMMT	X_M	20.00	29.00	32.00	48.00	55.00	67.00	75.00
	$N_{T\times}10^{15}$	1.34	1.95	2.17	3.28	3.77	4.60	5.11

$M_o = 0.495$ g cm^{-3}, *P* (St-*co*-BA), ($\rho_p = 1.07$ g cm^{-}3), *P* (St-*co*-BA) with OMMT, ($\rho_p = 1.09$ g cm^{-3}) and *P* (St-*co*-BA-*co*-Si) with OMMT, ($\rho_p = 1.12$ g cm^{-3})

absorption of the emulsion is far less than that of the uncomposite. In other words, the water resistance of the former is far better than that of the uncomposite. In addition, the water absorption can be decreased by increasing 4-MPMHS content, and also it can reach to the smallest when the content of OMMT is 1 wt %. This can be explained on the basis of intercalation of P (St-*co*-BA-*co*-Si) into the OMMT layers, making less room for water molecules. The higher OMMT concentration suppresses the intercalation and makes the framework of nanocomposite loose, which results in the water absorption increase. In addition, organic groups of 4-MPMHS arrange outwardly on the emulsoid particle. This could also enhance the water resistance for the emulsion film.

Surface tension of the emulsion

The surface tension (σ) was one of the important properties of the emulsion. The flow property and wetting property to base substrate were related to the surface tension. Table VI shows that the values of surface tension (25°C) of emulsion are enhanced with increase of 4-MPMHS content, and the value goes down to the smallest at 1 wt % of OMMT. Again, the surface tension of nanocomposite emulsion was lower in comparison with the silicone-acrylate emulsion. The surface tension of water is very big (72 mN m^{-1}), and far larger than wetting tension on substrates, therefore, one of the key elements for improving properties of emulsion was decreasing the surface tension. The equation describing surface tension was given by Young.[34]

$$\sigma_S = \sigma_{SL} + \sigma_L \cdot \cos\ \theta, \tag{8}$$

where σ_S and σ_L are surface tension of solid and liquid, respectively, σ_{SL} is the interface tension of solid–liquid, θ is contact angle. The smaller the value of θ; the better is the wetting property. Lower surface tension causes θ to become smaller, so it is of advantage that emulsion wetting to base substrate, increasing the adhesion outspreads on substrates, enhancing flowing leveling. Thus, it can be seen that the nanocomposite emulsion was superior to the silicone-acrylate emulsion in the surface tension, and the nanocomposite emulsion containing 1 wt % OMMT was the best.

Drying speed of the emulsion

Figure 12 shows that the drying speed of the nanocomposite emulsion was faster than that of the P (St-*co*-BA-*co*-Si) emulsion, and the nanocomposite emulsion containing 1 wt % OMMT was the fastest one. Water volatilization was related to the free volume of material and surface tension. The particle size of the nanocomposite emulsion is smaller, the free volume is bigger, therefore, vapor volatilize easily. In addition, the surface tension of nanocomposite is lower, the volatilization speed of

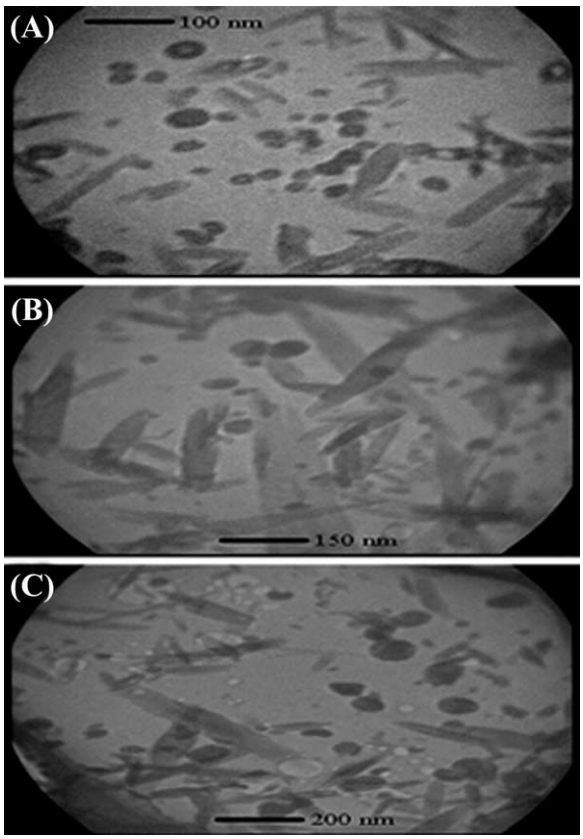

Figure 11 TEM micrographs of (A) P (St-*co*-BA), (B) P (St-*co*-BA) with OMMT and (C) P (St-*co*-BA- *co*-Si) with OMMT at 81°C.

TABLE V
Water Absorption of the Emulsion Film

No. of samples	Water absorption	No. of samples	Water absorption	No. of samples	Water absorption
1	0.1696	6	0.1370	11	0.1347
2	0.1140	7	0.1092	12	0.1064
3	0.1098	8	0.1030	13	0.1023
4	0.1182	9	0.1133	14	0.1080
5	0.1317	10	0.1150	15	0.1127

surface molecules is higher, and is dried more quickly. Higher drying speed is more advantageous in practice.

Thermal properties

The thermal properties of P (St-*co*-BA), P (St-*co*-BA) with OMMT and P (St-*co*-BA-*co*-Si) and OMMT with 1 wt % OMMT were evaluated by means of differential scanning calorimetry (DSC) and TGA/DTG under nitrogen atmosphere. DSC curve of the P (St-*co*-BA) reveals an endothermic shift around 101.19°C, which corresponds to T_g. The T_g is around 100.8°C, for P (St-*co*-BA) with OMMT and 8.964°C, for P (St-*co*-BA-*co*-Si) with OMMT thermograms, respectively. By addition of 4-MPMHS to copolymers, the T_g decreased drastically. The peak position related to the glass transition temperature (T_g) was higher in the order P (St-*co*-BA) > P (St-*co*-BA) with OMMT > P (St-*co*-BA-*co*-Si) with OMMT. The higher T_g for P (St-*co*-BA) was interpreted as being due to the effect of the more difficult micro Brownian motion of the stiffer chains rather than silicone containing polymer chains. According to these results, it is found that the presence of 4-MPMHS moiety causes the change in thermal behavior and it particularly affects T_g.

The TGA/DTG curve of the P (St-*co*-BA) shows a stable situation up to 250°C. The chemical decomposition will start after this temperature and the maximum decomposition is around 460°C. The P (St-*co*-BA) with OMMT emulsion shows a stable situation up to 264°C and the chemical decomposition will start after this temperature and the maximum decomposition is around 595°C. On the other hand, the P (St-*co*-BA-*co*-Si) with OMMT emulsion shows a stable situation up to 290°C and the chemical decomposition will start after this temperature and the maximum decomposition is around 482°C which is due to the presence of 4-MPMHS. According to these results, it can be concluded that the existence of 4-MPMHS moiety in the copolymers causes some thermal stability and by increasing the amount of silicone thermal stability increases.

TABLE VI
Surface Tension of Emulsion (mN m^{-1})

No. of samples	σ	No. of samples	σ	No. of samples	σ
1	34.0	6	34.9	11	36.9
2	31.8	7	34.3	12	35.2
3	31.2	8	32.0	13	33.3
4	32.1	9	32.3	14	33.9
5	33.1	10	33.9	15	34.1

CONCLUSIONS

A new silicone containing macromonomer, 4-(methacrylamido) phenoxy polymethylhydrosiloxane (4-MPMHS) with a vinyl group, has been synthesized for formulation of nanocomposite emulsion. Then Poly (styrene-*co*-silicone-*co*-butylacrylate) with organic modified montmorillonite nanocomposite emulsion were prepared by *in situ* intercalative emulsion polymerization of styrene (St), butyl acrylate (BA), and 4-MPMHS, in the presence of organic modified montmorillonite (OMMT) with different OMMT contents (0, 0.5, 1.0, 1.5, and 2 wt %). It is evident that the properties of silicone/styrene/butylacrylate emulsion were improved by the intercalative polymerization of butylacrylate, styrene and silicone in the presence of OMMT. The property of nanocomposite emulsion containing 1 wt % OMMT was the best one, and the following advantages were obtained: smaller particle size, faster drying speed, smaller surface tension, and improved resistance to water by the incorporation of OMMT.

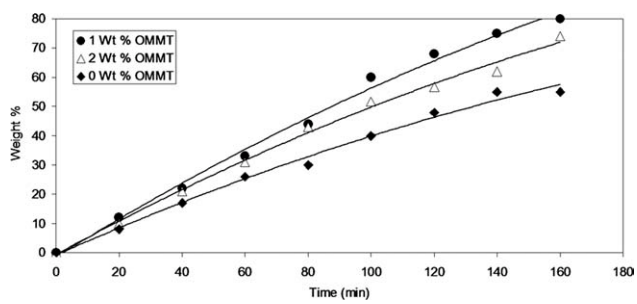

Figure 12 Drying speed graphs of emulsion containing 5 wt % 4-MPMHS and (◆) 0 wt % OMMT (●) 1 wt % OMMT, and (△) 2 wt % OMMT.

References

1. Huang, S. Q.; Peng, H.; Huang, H.; Li, S. B. N Chem Mater 1997, 9, 22.
2. Ma, W. S.; He, J. H.; Ou, Z. Y.; Pan, H. M. Paint Coat Ind 2003, 4, 1.
3. Wang, J.; Chu, F. X. China Adhes 2003, 5, 52.
4. Naghash, J. H.; Karimzadeh, A.; Massah, A. R. J Appl Polym Sci 2009, 112, 1037.
5. Naghash, J. H.; Mallakpour, S.; Forushani, Y. P.; Uyanik, N. Polymer (Korea) 2008, 32, 95.
6. Naghash, J. H.; Karimzadeh, A.; Momeni, A. R.; Massah, A. R.; Aliyan, H. Turk J Chem 2007, 31, 257.
7. Naghash, J. H.; Mallakpour, S.; Mokhtarian, N. Prog Org Coat 2006, 55, 375.
8. Naghash, J. H.; Mallakpour, S.; Kayhan, N. Iran Polym J 2005, 14, 211.
9. Naghash, J. H. Polymer (Korea) 2010, 34, 1.
10. Naghash, J. H. Massah, A. R.; Arman, M. Prog Org Coat 2009, 65, 275.
11. Bavon, L.; Wang, P. C.; Pinnavaia, T. Z. Appl Clay Sci 1999, 15, 11.
12. Okada, A.; Kawasami, M.; Usuki, A.; Kojima, Y.; Kamigaito, O. Mater Res Soc Proc 1990, 171, 45.
13. Shen, Z. Q.; Simon, G. P.; Cheng, Y. B. J Appl Polym Sci 2004, 94, 2101.
14. Messersmith, P. B.; Ciannelis, E. P. Chem Mater 1994, 6, 1719.
15. Hassan, M. A.; Kozlowski, R.; Obidzinski, B.; Shehata, A. B.; Aziz, F. A. Polym Plast Technol Eng 2007, 46, 521.
16. Rui, Z.; Yuan, H.; Jiayan, X.; Weicheng F.; Zuyao, C. Polym Degrad Stab 2004, 85, 583.
17. Wang, Y. Q.; Zhang, H. F.; Wu, Y. P. Eur Polym Mater 2005, 41, 2776.
18. Barmar, M.; Barikani, M.; Fereidounnia, M. Iran Polym J 2006, 15, 709.
19. Diaconu, G.; Asua, J. M.; Paulis, M.; Leiza, J. R. Macromol Symp 2007, 259, 305.
20. Patel, H. A.; Somani, R. J.; Bajaj, H. C.; Jasrva, R. V. Bull Mater Sci 2006, 29, 133.
21. Huang, X.; Lewis, S.; Brittain, W. J Macromolecules 2000, 33, 2000.
22. Kim, T. H.; Jang, L. W.; Lee, P. C.; Choi, H. J.; Jhon, M. S. Macromol Rapid Commun 2002, 23, 191.
23. Li, X.; Ha, C. S. J Appl Polym Sci 2003, 87, 1901.
24. Chin, I.; Albrecht, T. T.; Kim, H.; Russell T. P.; Wang, J. Polymer 2001, 42, 5947.
25. Liang, Y.; Jia, D.; Zhou, Y.; Du, M.; Huang, A. Paint Coat Ind 2004, 5, 11.
26. Feng, X.; Zhong, A.; Chen, D. J Appl Polym Sci 2006, 101, 3963.
27. Kumar, P. N.; Paresh Sanghvi, G. S.; Shah, D. O.; Surekha, D. Langmuir 2000, 16, 5864.
28. Badran, A. S.; Moustafa, A. B.; Yehia, A. A.; Shendy, S. M. M. J Polym Sci A Polym Chem 1990, 28, 411.
29. Lambourne, R. Paint and Surface Coatings Theory and Practice; Ellis Horwood Market Cross House: Chichester, 1987, Chapter 9, p 59.
30. Ba, Y.; Ratcliffe, C. I.; Ripmeester, J. A. Adv Mater 2000, 12, 603.
31. Sadhu, S.; Bhowmick, A. K. J Appl Polym Sci 2004, 92, 698.
32. Hinds, W. C. Aerosol Technology, 2nd ed.; Wiley: New York, 1999; Chapter 4.
33. Chinwanitcharoen, C.; Kanoh, S.; Yamada, T.; Hayashi, S.; Sugano, S. J Appl Polym Sci 2004, 91, 3455.
34. Adamson, A. Physical Chemistry of Surfaces, 5th ed.; Wiley: New York, 1990; Chapter 10.